Assessing Videogrammetric Techniques for Measuring High Aspect Ratio Wing Deflection in Wind Tunnel Application

Norzaima Nordin
Department of Aeronautic Engineering and Aviation, Faculty of Engineering, Universiti Pertahanan Nasional Malaysia

Mohammad Yazdi Harmin
Department of Aerospace Engineering, Faculty of Engineering, Universiti Putra Malaysia

https://doi.org/10.5109/7323253

出版情報：Proceedings of International Exchange and Innovation Conference on Engineering & Sciences (IEICES). 10, pp.128-134, 2024-10-17. International Exchange and Innovation Conference on Engineering & Sciences
バージョン：

Assessing Videogrammetric Techniques for Measuring High Aspect Ratio Wing Deflection in Wind Tunnel Application

Norzaima Nordin[1], Mohammad Yazdi Harmin[2]
[1]Department of Aeronautic Engineering and Aviation, Faculty of Engineering, Universiti Pertahanan Nasional Malaysia, 57000 Sungai Besi, Kuala Lumpur, Malaysia, [2]Department of Aerospace Engineering, Faculty of Engineering, Universiti Putra Malaysia, 43400 Serdang, Selangor, Malaysia.
norzaima@upnm.edu.my

Abstract: *High aspect ratio (HAR) wings present remarkable aerodynamic benefits, characterized by high lift and low induced drag. Nonetheless, the flexibility of these wings causes significant deformations and nonlinear responses, making accurate prediction essential for understanding HAR wing behavior. Although nonlinear geometrical models have been developed, validation of HAR wings remains limited. Previous experimental approaches have primarily used contact methods, which are unsuitable for HAR wings as it alters the mass and stiffness of the structure. To address this limitation, this study proposes a non-contact videogrammetric measurement technique employing an ultrahigh-speed camera for motion capture. A new approach using a z-indicator is proposed to measure wing deformation. The experiment was performed with five configurations of effective angle of attack (AoA) in the wind tunnel test, predicting three-axis wing deflections. The experimental data were validated using conventional and combined modal finite element methods.*

Keywords: High aspect ratio; Videogrammetric measurement technique, Wind tunnel test; Wing deformation

1. INTRODUCTION

The aircraft wing serves as the primary structural component responsible for lift generation, enduring nearly all applied loads. Throughout the wing design process, engineers rely on approximate analytical models to predict wing bending and twist under aerodynamic loads. However, these models often prove inadequate in accurately predicting the actual deflections experienced by aircraft wings under real flight conditions. Comparison studies with observed wing deformations in various flight conditions are essential to improve the reliability of these analytical models. Among the techniques used for such comparison studies is the wind tunnel test [1-4].

Several techniques have been used to measure model deformation and aeroelastic behaviour in the wind tunnel test. One of the well-known techniques implemented is using the videogrammetric model deformation (VMD) measurement technique [5-10]. As it is a non-contact method and does not alter the mass or wing model stiffness, this measurement technique is deemed fitting for flexible wing structures. This measurement technique depends on the optical method for measuring aeroelastic deformation in the wind tunnel. It involves the application of a single-camera or a multiple-camera approach. In most cases, a single-camera approach is used for a single-view measurement approach to determine two of the three in xyz unknown coordinates. For this approach, one of the three target coordinates must be known in order to calculate the remaining two unknowns. However, if all three target coordinates are unknown, the multiple-camera approach based on a 3D photogrammetric collinearity equation is considered. This multiple-camera approach is commonly used in the wind tunnel test, as it is not feasible to determine the single unknown coordinate. Otherwise, if one of the three target coordinates is known, the single-camera approach is sufficient to control the limited access of camera-viewing points and undesirable glares. In such a scenario, the use of multiple cameras causes uncertainty in the ensuing measurement. Burner and Liu [5] proposed the use of a single-camera VMD system and set it up with a charge-coupled device (CCD) camera, a computer with image acquisition and a light source for the target placed on a wing model. For the calculation of the bending and twist deflections of the wing model, the study applied a linear fitting method (for twist calculation according to the local angle of attack that fits the target coordinate in x-plane and z-plane) and least-square method (for determination of wing bending deflection). In addition, the study fixed a spanwise location to reduce the unknown number and used the single-camera VMD to determine the remaining two object-space coordinates. Barrows [11] incorporated the same technique with passive and active targeting using photogrammetry and projection moiré interferometry (PMI). The retro-reflective target (passive target) was placed on the wing element, which served as a baseline for the comparison of results between the condition of wind-off and wind-on in the wind tunnel test. The wing bending deflection was calculated using the single-camera photogrammetric technique. Meanwhile, Pitcher et al. [12] applied the VMD technique to examine the wing motion of the flexible Nighthawk mini-UAV. The standard VMD technique was extended to the resonance shape and spectral analysis of the flapping behaviour of the wing model. A non-coded target in circular dots and a coded target surrounded by banded sections were subjected to the wind tunnel test. Three synchronised digital cameras were used; each camera captured a maximum of 75 frames per second at 1280 × 1024 pixels. The results revealed flutter behaviour at a negative angle of attack and highlighted the need for a higher frame rate to expand the dynamic range of the measurement and observe the aeroelastic response of the wing.

Accordingly, the process of calibrating the camera is pivotal in the videogrammetric measurement technique. The location of the principal point, the focal length (zoom) and de-centre camera lens distortion was calculated during the calibration process. Following that, the camera is positioned to capture the image sets with the identified targets. In order to capture high-quality images, it is necessary to have proper lighting that illuminates high-contrast targets without producing glare off the wing, the wind-tunnel viewing glass, or the wind-tunnel floor that may wash out the targets or cause false targets. The location of each target within each frame is then exported to a data file. Zhang et al. [13] applied a similar approach to supersonic wind tunnel facilities. The study set up two cameras with 4,000,000 pixels and a fixed focus lens was used to accommodate a videogrammetric system. The measurement of deflection displacement vector calculation was based on a photogrammetric collinear equation which expresses in Eq. (1) and (2) [13]:

$$(x) + f\,\frac{a_1(X - X_s) + b_1(Y - Y_s) + c_1(Z - Z_s)}{a_3(X - X_s) + b_3(Y - Y_s) + c_3(Z - Z_s)} = x_p \quad (1)$$

$$(y) + f\,\frac{a_2(X - X_s) + b_2(Y - Y_s) + c_2(Z - Z_s)}{a_3(X - X_s) + b_3(Y - Y_s) + c_3(Z - Z_s)} = y_p \quad (2)$$

where $a_1, a_2, a_3, b_1, b_2, b_3, c_1, c_2, c_3$ is the element of rotation matrix determined by camera altitude, x_p, y_p is the centre coordinate of camera image plane, X_s, Y_s, Z_s is the coordinates of camera centre in 3-D, f is the camera focal length, x, y, z is the measuring coordinate in 2-D and X, Y, Z is the measuring coordinate in 3-D.

However, prior studies mainly focused on the low aspect ratio (LAR) wing. Only a few studies on the HAR wing applications considered the VMD measurement technique. For instance, Tang and Patil [14,15] considered the attachment of the HAR wing to a slender body to explore its aeroelastic response. The study applied the contact-method approach with axial strain gauges and 45° angle oriented strain gauges for bending and torsional modes, respectively. Besides that, the study proceeded to mount a micro accelerometer at the midspan of the wing, which served as an input for the transfer function analysis. A mirror deflection technique was applied to measure the tip static aeroelastic deflections by attaching a mirror to the wing. Meanwhile, focusing on the geometrical nonlinearity of the HAR wing, Qian et al. [16] conducted an aeroelastic wind tunnel test to measure the wing deformation based on a VMD measurement system. For this, the study installed two cameras at the upper panel experimental section for the collection and processing of deformation data.

Despite the extensive literature on the VMD measurement technique, the details of conducting an experiment involving the HAR wing model under the undeformed configuration have remained scarce. The undeformed configuration overlooks the gravitational loading effect. For the single-camera approach, prior studies did not clearly state the required measurement technique. Moreover, only a few studies reported the validation of the experimental data with the numerical model. Therefore, based on the identified gaps in the existing literature, this paper will propose a non-contact videogrammetric measurement technique employing an ultrahigh-speed camera for HAR wing deflection under the undeformed configuration in the wind tunnel test application.

2. METHODOLOGY

The wind tunnel test was primarily conducted to examine and validate the bending characteristics (in terms of displacement) obtained from conventional finite element (FE) and combined modal finite element (CMFE) performed by Nordin et al. [17,18]. The experiment was conducted in a closed loop wind tunnel (CLWT) located in the Aero-Lab Shelter of Aerospace Engineering, Universiti Putra Malaysia using videogrammetric measurement techniques via an ultrahigh-speed camera. In order to ensure the precision of the results, this experimental work started with the wind tunnel calibration, followed by the insertion of the wing model and the wind tunnel setup including wing model setup, zeroing angle identification and ultrahigh-speed camera arrangement.

2.1 Wind Tunnel Setup

The wing was setup as an undeformed configuration (exclusion of gravitational loading effect), vertically fixed at the rotating wing root mechanism at the top of the test section. The wing models with aspect ratios, AR-16 are used for this paper. The model consists of three components: the spar, ribs and fairing, based on the wing model validated by Nordin et al. [19] as shown in Fig.1.

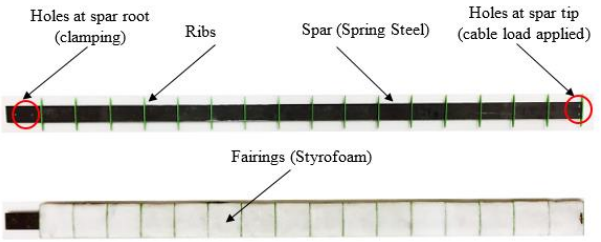

Fig. 1. Fabrication of rectangular HAR wing model.

The tracking points were marked on the top surface of the wing, faced to the ultrahigh-speed camera for movement tracking record. A speed index marking and z-axis indicator scale also facilitated the setup, which served as a reference during the execution of the test. The adjustable rotating mechanism at the top of the wind tunnel section was purposely designed to fix the wing root model. This allowed the rotating adjustment of the desired effective angle of attack. The mechanism must be adjusted for zeroing angle identification prior to running the test. The effective angle of attack was indicated by the protractor angle ruler mounted on top of the rotating disc. In order to set for zero effective angle of attack, the angle handle was adjusted until the pointer was placed to zero on the protractor. Once set, the centre locking system was fastened to ensure that this position was immovable despite the applied loads. This fixture was pre-tested by running up the wind tunnel in order to observe the responses of the wing model with the changing speed. The test was allowed to proceed when the wing model was not deflected at zero angle considering that neither change on lift nor pressure distribution was achieved when the speed increased.

The effective angle of attack, AoA is initially set at the range of AoA 1° to AoA 5°. Fig. 2 illustrates the details angle of attack where effective AoA or known as α_{eff} can be defined as the angle at which the local relative wind strikes to the airfoil or wing of an aircraft. In this study, the effective angle of attack angle is set up to maximum value (AoA 5°), taking into consideration the aeroelastic condition, which result in additional twist deflection (known as a pitch angle or induced angle of attack, α_i) due to aeroelastic effect. This leads to a higher geometric angle of attack, α as the velocity increases.

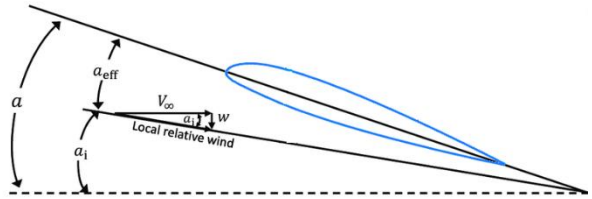

Fig. 2. Geometric, induced and effective angle of attack.

The Phantom ultrahigh-speed camera [20] was used to capture the movement of the wing model during the wind tunnel test. The camera was positioned to align the z-axis reference of the wing in order to record the motion of each tracking point as shown in Fig.3. The PCC software in the laptop linked to the camera was used to obtain the deformation of each tracking point. The setup for the wind tunnel test involved: (a) pre-installation process, (b) calibration process and (c) capturing wing motion via PCC software.

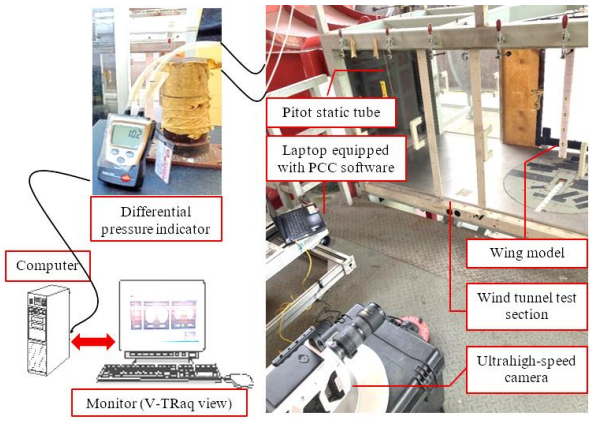

Fig. 3. Wind tunnel setup with velocity tunnel reference acquisition (V-TRAq) software and ultrahigh-speed camera using PCC software.

Pre-installation process

In this phase, the Phantom camera was connected to the host laptop using an ethernet LAN connection. The position of the camera was adjusted to provide a clear view of the wing model in the PCC software. For the software, a similar IP address was set. At the same time, the wind tunnel was turned on, and the airspeed was controlled by a host computer equipped with the V-TRAQ software.

Calibration Process

An ultrahigh-speed camera was used to carry out the calibration process. This process is crucial to ensure accurate measurement during the test. Prior to the measurement process, calibration was used to scale the image size in meter per pixel (m/pix). The calibration process in this study required using two points separated by a defined distance. The distance between the two selected points was inserted into the PCC software, which scaled the image from the captured video. For this study, the scale was set at 0.0005198 m/pix with the calibration error ± 0.0055 m. A few markings are to be set during the calibration procedure to track the distance between points.

Capturing wing motion via PCC software

In order to acquire the high-quality and clear video, the camera specifications must be set up from the PCC software, in correspondence to the surroundings before capturing the motion of the wing. A higher resolution was deemed necessary in this study, as a wider image was required to view the tracking points placed on the wing model. The frame per second (fps) was set relatively high to obtain a clear view of the wing motion since the wing can deflect in a split second.

As the experiment was conducted in low-light conditions, the exposure time was set to be relatively long. The process of capturing wing motion began by clicking on the capture button in the PCC software, which put the Phantom camera into record mode. A trigger button was pressed to start and stop recording. The video was analysed once it was recorded to obtain the actual data (in 2-D). The wing model was marked with four tracking points to observe the deflection.

Fig. 4 shows the motion of the wing that is being captured using PCC software. The recorded video of the wing deflection was subsequently saved in the .cine file format. The same procedure was repeated for a range of effective angle of attack, starting from AoA 1° to AoA 5°.

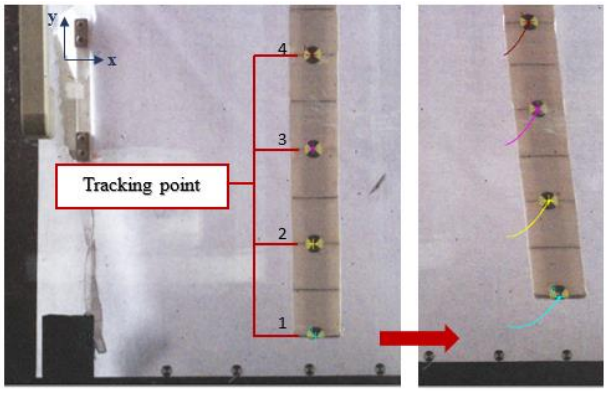

(a) start (b) end

Fig. 4. Snapshot tracking point of video processing.

2.2 Measurement and Data Collection

The PCC software is a 2-D motion analysis that can only compute and measure xy-coordinates. In this work, the measurement of the y-direction was considered and the data was utilised to determine the wing deflection in the z-direction using the linear interpolation method. The measurement started with the selection of tracking points along spanwise before the wing began to deflect. The video was played until the wing started to flutter. The collected data were subsequently saved and analysed.

Throughout the data collection, the coordinates of the tracking points were retrieved from the recorded video and converted to the desired format. The data is then tabulated depending on the image frame, which is based on the wind tunnel speed. The displacement of the wing deflection was calculated by subtracting the coordinate after the wing deflected from its original location at zero airspeed. Eq. (3) expressed the linear interpolation formula to determine y-deflection of the rectangular HAR wing according to the airspeed required.

$$y_2 = \left[\left(\frac{v_2 - v_1}{v_3 - v_1}\right) \times (y_3 - y_1)\right] + y_1 \quad (3)$$

where y_1 is the *y*-deflection at the lower region, y_2 is the *y*-deflection at speed required, y_3 is the *y*-deflection at the upper region, v_1 is the speed at the lower region, v_2 is the speed required and v_3 is the speed at the upper region. The reported tip deflection values were obtained by averaging measurements taken at three different instances. This approach was chosen to ensure accuracy and reliability in the data, as well as to reduce the impact of any irregularities occur in a single measurement.

2.3 Determination of Z-indicator in Wind Tunnel

This subsection describes a new method of identifying z-direction. The initial measurement of z-direction (known as z-indicator) was required and performed in the wind-off condition. This z-indicator served as a reference to determine the z-deflection in this study. The top and bottom walls of the wind tunnel section were uniformly marked 5 cm apart from the wing until 40 cm behind the deflection path of the wing. Ropes were attached vertically at each marking point, as shown in the Fig. 5. Due to the size constraints of the wind tunnel section, the maximum marking was approximately 40 cm in order to prevent any damage at the test section. The method used to determine y-deflection was identical to the method discussed in the preceding subsection. The wing was pushed manually until it aligned with the marker. The wing movement was then recorded via PCC software. These steps continued until it reached 40 cm. After the extraction of z-indicator data, the value of y-deflection data obtained in the preceding steps was interpolated with the z-indicator data in order to obtain the value of z-deflection. The deflections value in z-direction were determined based on the interpolation method using the Eq. (4) prior to the validation with the conventional FE simulation result of nonlinear static analysis.

$$z = \left[\left(\frac{y - y_1}{y_2 - y_1}\right) \times (z_2 - z_1)\right] + z_1 \quad (4)$$

where z is the unknown deflection in the z-direction, y is the deflection in the *y*-direction, y_1 is the *y*-deflection at the upper region (based on *z*-indicator), y_2 is the *y*-deflection at the lower region (based on *z*-indicator), z_1 is the *z*-indicator at the upper region and z_2 is the *z*-indicator at the lower region.

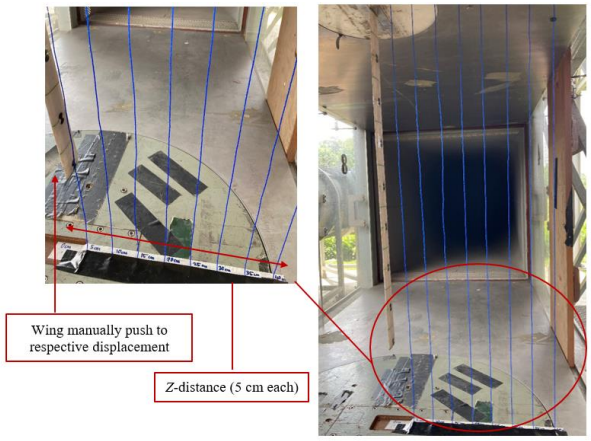

Fig. 5. Determination of z-indicator in wind tunnel test section.

3. RESULTS AND DISCUSSIONS

In experimental work, it is important to make an assessment of data accuracy. Therefore, the current experiment performed three (3) repeat runs for all five configurations effective angle of attack in the wind tunnel test. Fig. 6 presents the graph deflections in a y-direction between simulation results (via CMFE and FE) and experimental data using the ultrahigh-speed camera at a different range of velocities and effective angle of attack.

As observed in Fig. 6, the agreements between different results are quite satisfactory. The result of this experiment shows an almost identical graph pattern to CMFE and FE when the velocity increases. CMFE and FE show almost similar results at the attack angle, AoA 1° to AoA 3°. The difference between both approaches observed clearly diverge starting at AoA 4° and AoA 5°.

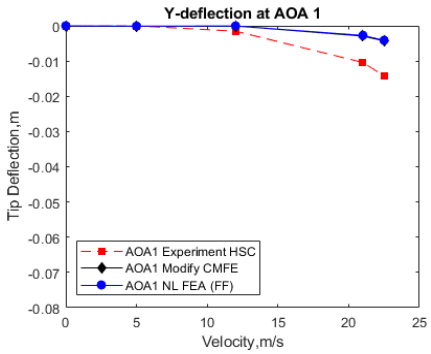

(a) AoA 1°

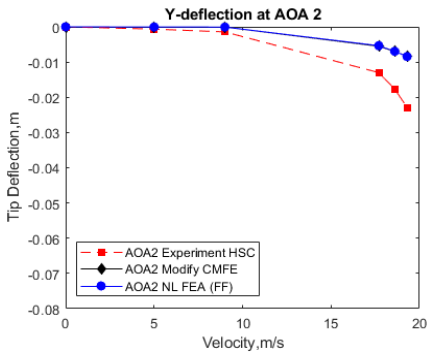

(b) AoA 2°

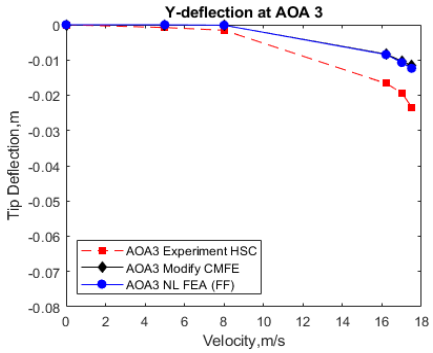

(c) AoA 3°

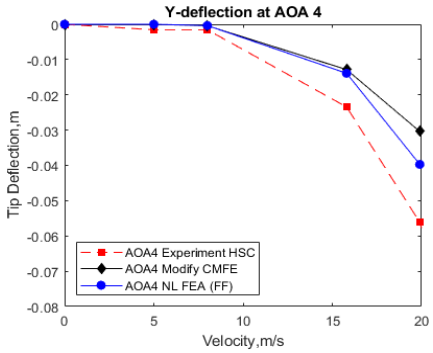

(d) AoA 4°

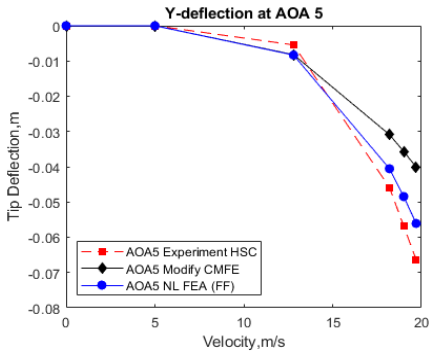

(e) AoA 5°

Fig. 6. Comparison *y*-deflection data.

Table 1 presents the differences between the results obtained from the conventional FE, CMFE and experimental approaches in term of displacement (measured in meters). The highest deflection difference between the CMFE and experimental data was only 2 cm at the velocity of 19.7 m/s at effective angle of attack, AoA 5°.

Measuring of y-deflection may be impacted by various sources of error, including random errors stemming from unpredictable fluctuation in the measurement process such as vibrations, humidity and temperature. To mitigate these errors, multiple measurements were conducted and the average value was plotted as the final data. In addition, systematic errors can arise from flaws in the experimental setup such as wing condition and position. To minimise the impact of these errors, certain actions must be taken to ensure the wing is in optimal condition and positioned correctly in order to achieve consistency in the measurements.

Table 1. *Y*-deflection difference with CMFE and FEA

AoA (°)	Speed (m/s)	Y-tip deflection (m)			CMFE vs Exp
		FEA	CMFE	Exp	Diff (m)
1	22.5	-0.0041	-0.0043	-0.0142	0.0099
2	18.6	-0.0084	-0.0083	-0.0229	0.0146
3	17.5	-0.0124	-0.0116	-0.0234	0.0118
4	20.4	-0.0442	-0.0331	-0.056	0.0229
5	19.7	-0.0560	-0.0400	-0.0663	0.0263

The deflection value of z-deflections was calculated based on the interpolation formula expressed in the Eq. (4). As shown in Fig. 7 and Table 2, the agreements between different results are quite acceptable. The result of this experiment shows an almost similar graph pattern to CMFE and conventional FE when the velocity increases. Most of the z-deflections via CMFE show the highest result, followed by conventional FE and experimental results. The maximum tip deflection difference between CMFE and experimental data is approximately only 1.7 cm at the effective angle of attack, AoA 3°.

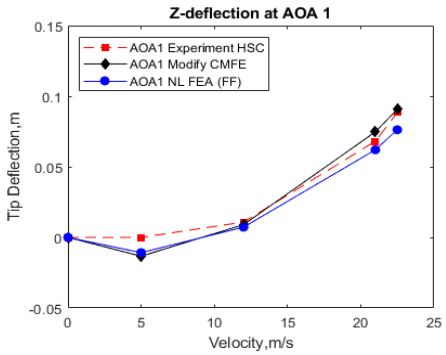

(a) AoA 1°

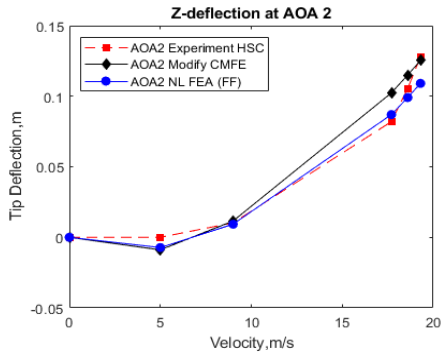

(b) AoA 2°

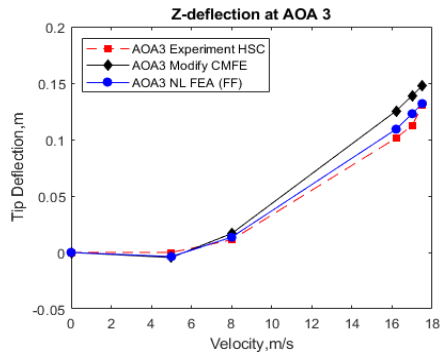

(c) AoA 3°

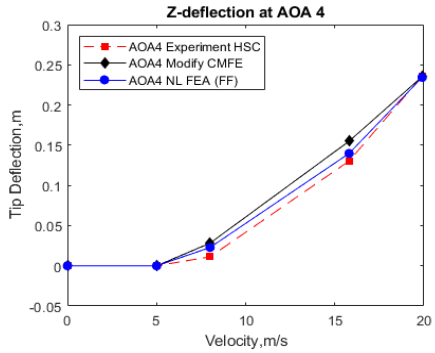

(d) AoA 4°

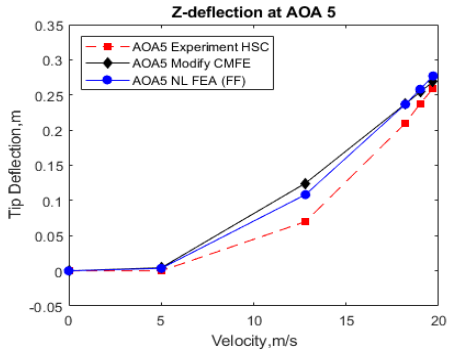

(e) AoA 5°

Fig. 7. Comparison *z*-deflection data.

Table 2. *Z*-deflection difference with CMFE and FEA

AoA (°)	Speed (m/s)	Z-tip deflection (m)			CMFE vs Exp	
		FEA	CMFE	Exp	Diff (m)	Diff %
1	22.5	0.0760	0.0907	0.088	0.002	2.60
2	18.6	0.1090	0.1253	0.127	0.002	2.03
3	17.5	0.1318	0.1475	0.130	0.017	13.2
4	20.4	0.2469	0.2453	0.254	0.009	3.58
5	19.7	0.2770	0.2689	0.259	0.009	3.78

However, the result from experimental data is relatively low at the highest effective angle of attack compared to other approaches. This is due to some uncertainties that are based on wind tunnel vibrations during testing, which can potentially cause unsynchronised configuration setups of ultrahigh-speed camera. Furthermore, human errors such as errors in reading and recording data, changes in the effective angle of attack at the rotating root mechanism were also considered and addressed during the experiment. Additional uncertainty considerations must be taken into account, including the effect of changes in the deflection in the x-direction. As mentioned earlier, the predicted deflection in x-direction using CMFE and conventional FE methods showed nearly zero deflection. However, in the wind tunnel test revealed a slight deflection of approximately 0.004 m in the x-direction. Fig. 8 shows a comparison of sample deflections in the x-direction at effective angle of attack, AoA 3°. This deflection may have occurred due to the wing clamping conditions, which were unable to hold the wing tighly at higher velocities and resulted in a slight chordwise-bending deflection toward the rectangular HAR wing model.

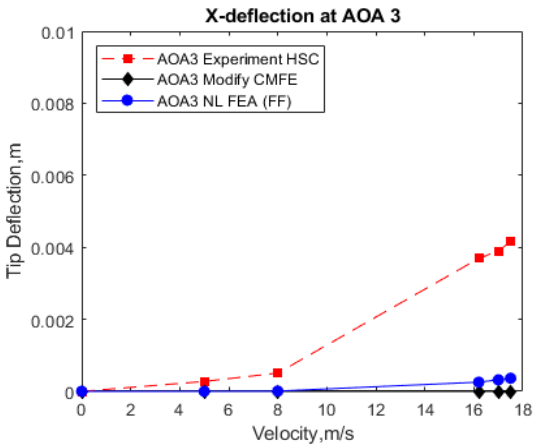

Fig. 8. Tip deflection in the *x*-direction (AoA 3°).

4. CONCLUSION

In summary, the comparative analysis of *z*-direction data between the CMFE and the conventional FE, and wind tunnel test results reveals a closely aligned pattern with minimal percentage differences. This alignment underscores the practicality and accuracy of the videogrammetric measurement technique in determining displacement. Specifically, the technique demonstrated remarkable precision for the rectangular HAR wing, showing a variance of only 4 mm in the *x*-direction and *z*-direction is less than 13.2% compared to simulation results. Furthermore, the use of an ultrahigh-speed camera was instrumental in capturing the dynamic phenomena occurring during the experiments, providing detailed insights into the wing's behavior under various conditions. This capability is crucial for understanding and analyzing rapid movements and deflections that occur in high-speed aerodynamic testing environments. The introduction of the z-indicator as a reference point for measuring deflection in the rectangular HAR wing marks a significant advancement in videogrammetric measurement techniques. This innovative approach not only enhances the accuracy of displacement measurements but also simplifies the process, offering a new approach for future wind tunnel testing applications.

5. REFERENCES

[1] Lizotte A. M., and Lokos, W. A, Deflection-Based Aircraft Structural Loads Estimation with Comparison to Flight, AIAA/ASME/ASCE/AHS/ ASC Struct. Dyn. Mater. Conf, vol. 4 (2005) 2698–2715.

[2] Northington, J. S. and Pasiliao, C. L, F-16 Wing Structural Deflection Testing - Phase I, AIAA J., vol. 1674 (2007) 648–663.

[3] Gharibi, A., Ovesy, H. R. and Khaki, R., Development of Wing Deflection Assessment Methods Through Experimental Ground Tests and Finite Element Analysis, Thin-Walled Struct., vol. 108 (2016) 215–224.

[4] Harmin, M. Y., and Cooper, J. E., Aeroelastic Behaviour of a Wing Including Geometric Nonlinearities, Aeronaut. J., vol. 115, no. 1174 (2011) 767–777.

[5] A. W. Burner and T. Liu, Videogrammetric Model Deformation Measurement Technique, J. Aircr., vol. 38, no. 4 (2001) 745–754.

[6] E. Germain and J. Quest, The Development and Application of Optical Measurement Techniques for High Reynolds Number Testing in Cryogenic Environment, 43rd AIAA Aerosp. Sci. Meet. Exhib., (2025) 1–9.

[7] A. W. Burner, G. A. Fleming and J. C. Hoppe, Comparison of Three Optical Methods for Measuring Model Deformation, 38th Aerosp. Sci. Meet. Exhib., (2000).

[8] C. V. Spain et al., Assessing Videogrammetry for Static Aeroelastic Testing of a Wind-Tunnel Model," AIAA/ASME/ASCE/AHS/ASC Structure, Structural Dynamics and Materials Conference, vol. 3 (2024) 1824–1833.

[9] Rimi, Nasrin K., Rahman M. S. and Sadi T., Optimizing Aerodynamic Performance of Selig S3014 Airfoil through Dimensional Parametric Analysis, Proceedings of 9th International Exchange and Innovation Conference on Engineering & Sciences (IEICES), vol 9 (2023) 1-5.

[10] Bao, Hoang C., Khoa N. D., Quang H. M, Chieu T. H, and Phuong N. L, Application of Computational Fluid Dynamics in Examining the Filtration Efficacy of Fine and Coarse Particles in a Baffle Integrated-Vertical Ventilation Duct, Proceedings of 8th International Exchange and Innovation Conference on Engineering & Sciences (IEICES), vol 8 (2022) 259-264.

[11] D. Barrows, Videogrammetric Model Deformation Measurement Technique for Wind Tunnel Applications, 45th AIAA Aerosp. Sci. Meet. Exhib., vol. 38, no. 4 (2007) 745–754.

[12] N. Pitcher, J. Black, M. Reeder, and R. Maple, Videogrammetry Dynamics Measurements of a Lightweight Flexible Wing in a Wind Tunnel, 50th AIAA Struct. Struct. Dyn. Mater. Conf., (2019) 1–15.

[13] Z. Y. Zhang, X. H. Huang, J. Yin, and H. X. Lai, Videogrammetric techniques for wind tunnel testing and applications, Adv. Mater. Res., vol. 986–987 (2014) 1629–1633.

[14] D. Tang and E. H. Dowell, Experimental and Theoretical Study on Aeroelastic Response of High-Aspect-Ratio Wings, vol. 39, no. 8 (2001).

[15] Patil MJ, Hodges DH, On the Importance of Aerodynamic and Structural Geometrical Nonlinearities in Aeroelastic Behavior of High-Aspect-Ratio Wings, Journal of Fluids and Structures, vol. 19, no. 7 (2004) 905-915.

[16] W. Qian, Y. Bai, H. Zeng, and R. Yang, "Aeroelastic Wind Tunnel Experiment of a High-Aspect-Ratio Wing Model against Geometrical Nonlinearity, 31st Congr. Int. Counc. Aeronaut. Sci. ICAS (2018) 1–6.

[17] Nordin N., Bohari B., Chandrasegaran T., As'array. A and Harmin M. Y. Load Case Selection Technique for Combined Modal Finite Element Approach of High Aspect Ratio Wing Models, Journal of Aeronautics, Astronautics and Aviation 55, no. 3S (2023) 425-437.

[18] Nordin N, Chandrasegaran T and Harmin M. Y., Nonlinear Reduced Order Model of Rectangular High Aspect Ratio Wing with and without Follower Force Effects, Journal of Advanced Research in Fluid Mechanics and Thermal Sciences, vol. 63, no. 1, (2019) 117-134.

[19] Nordin, N., Rafi, N. S. M., and Harmin, M. Y., Nonlinear Follower Force Analysis with Ground Static Test Validation of High Aspect Ratio Wing, Lect. Notes Mech. Eng. (2020) 421–432.

[20] Vision Research Inc., Phantom ultrahigh-speed cameras v2511/ v2011/ v1611/ v1211, 2014.